Stress-dependent dynamic and reversible formation of cytoskeleton-like filaments and gel-transition by tardigrade tolerance proteins

Akihiro Tanaka[1], Tomomi Nakano[1], Kento Watanabe[1], Kazutoshi Masuda[2], Shuichi Kamata[1], Reitaro Yasui,[1] Hiroko Kozuka-Hata[3], Chiho Watanabe[2, #a], Takumi Chinen[4], Daiju Kitagawa[4], Masaaki Oyama[3], Miho Yanagisawa[2], Takekazu Kunieda[1*]

Affiliations

[1] Department of Biological Sciences, Graduate School of Science, The University of Tokyo, Bunkyo-ku, Tokyo, Japan

[2] Komaba Institute for Science, Graduate School of Arts and Sciences, The University of Tokyo, Meguro-ku, Tokyo, Japan

[3] Medical Proteomics Laboratory, The Institute of Medical Science, The University of Tokyo, Minato-ku, Tokyo, Japan

[4] Department of Physiological Chemistry, Graduate School of Pharmaceutical Sciences, The University of Tokyo, Bunkyo-ku, Tokyo, Japan

[#a] Current address: Graduate School of Integrated Sciences for Life, School of Integrated Arts and Sciences, Hiroshima University, Higashi-Hiroshima, Hiroshima, Japan.

* Corresponding author

Takekazu Kunieda

E-mail: kunieda@bs.s.u-tokyo.ac.jp

Abstract

Tardigrades are able to tolerate almost complete dehydration by entering a reversible ametabolic state called anhydrobiosis and resume their animation upon rehydration. Dehydrated tardigrades are exceptionally stable and withstand various physical extremes. Although trehalose and late embryogenesis abundant (LEA) proteins have been extensively studied as potent protectants against dehydration in other anhydrobiotic organisms, tardigrades produce high amounts of tardigrade-unique protective cytoplasmic-abundant heat-soluble (CAHS) proteins which are essential for the anhydrobiotic survival of tardigrades. However, the precise mechanisms of their action in this protective role are not fully understood. In the present study, we first postulated the presence of tolerance proteins that form protective condensates via phase separation in a stress-dependent manner and searched for tardigrade proteins that reversibly form condensates upon dehydration-like stress. Through comprehensive analysis, we identified 336 such proteins, collectively dubbed “dehydration-induced reversibly condensing proteins (DRPs)”. Unexpectedly, we rediscovered CAHS proteins as highly enriched in DRPs, 3 of which were major components of DRPs. We revealed that these CAHS proteins reversibly polymerize into many cytoskeleton-like filaments depending on hyperosmotic stress in cultured cells and undergo reversible gel-transition *in vitro*, which increases the mechanical strength of cell-like microdroplets. The conserved putative helical C-terminal region is necessary and sufficient for filament formation by CAHS proteins, and mutations disrupting the secondary structure of this region impaired both the filament formation and the gel transition. On the basis of these results, we propose that CAHS proteins are novel cytoskeletal proteins that form filamentous networks and undergo gel-transition in a stress-dependent manner to provide on-demand physical stabilization of cell integrity against deformative forces during dehydration and contribute to the exceptional stability of dehydrated tardigrades.

Introduction

Water is an essential molecule for maintaining the metabolic activity and cellular integrity of living organisms. Some organisms, however, can tolerate almost complete dehydration by entering a reversible ametabolic state called anhydrobiosis [1]. Tardigrades, also known as water bears, are a prominent example of such desiccation-tolerant animals [2]. Under a drying environment, tardigrades gradually lose almost all body water and concurrently contract their bodies to a shrunken round form called a tun. Dehydrated tardigrades are exceptionally stable and can withstand various physically extreme environments including exposure to space [3,4]. Even after exposure to extreme stressors, tardigrades can reanimate within a few dozen minutes after rehydration.

Several tolerance molecules against dehydration stress have been identified in various organisms. One of the most analyzed molecules is the non-reducing disaccharide, trehalose. A significant amount of trehalose accumulates during desiccation in several anhydrobiotic animals, such as sleeping chironomids [5], brine shrimp [6], and some nematodes [7], some of which require trehalose synthesis for anhydrobiotic survival [8]. Trehalose is proposed to play its protective roles through 2 modes of action: water replacement, in which trehalose substitutes for water molecules; and vitrification, in which trehalose preserves cell components in an amorphous solid (glassy) state [9]. In tardigrades, however, no or only a little trehalose accumulation occurs, even in dehydrated states of the anhydrobiotic species [10], and a recent study suggested that trehalose synthesis genes in tardigrades are acquired in only limited lineages via horizontal transfer after the establishment of their anhydrobiotic ability [11], suggesting the presence of a trehalose-independent anhydrobiosis mechanism in tardigrades.

Late embryogenesis abundant (LEA) proteins are another example of tolerance molecules. LEA proteins are principally unstructured proteins originally identified in desiccating plant seeds and later found in several anhydrobiotic animals [12]. LEA proteins have many proposed roles, including stabilization of vitrified trehalose, molecular shielding of client biomolecules, and sequestration of ions [12]. LEA proteins can suppress dehydration-dependent denaturation of enzymes, and have strong synergistic protective effects with trehalose [13]. The LEA proteins of brine shrimp were recently

reported to undergo phase separation to form droplet condensates upon dehydration and to increase the desiccation tolerance of insect cells [14].

Tardigrades produce a remarkable amount of tardigrade-unique cytoplasmic-abundant heat-soluble (CAHS) proteins rather than trehalose and LEA proteins [15]. CAHS proteins were originally identified in one of the toughest tardigrade species, *Ramazzottius varieornatus*, through a search for LEA-like heat-soluble proteins that remain soluble even after boiling [16]. Despite the absence of sequence similarity between CAHS and LEA proteins, these proteins share similar biochemical properties, e.g., high-hydrophilicity supporting heat-solubility and structural transition from the disordered state in hydration to a helix under desolvating or dehydrated conditions [12,16]. Like LEA proteins, CAHS proteins can protect enzymes from dehydration stress [17]. Knockdown of several CAHS genes that impaired the anhydrobiotic survival of tardigrades revealed that CAHS proteins are involved in the desiccation tolerance of tardigrades [17]. Although CAHS proteins were proposed to act as a vitrifying agent based on a shift in differential scanning calorimetry, this hypothesis was recently counter-argued as such a shift could be explained by the evaporation of residual water [18], and thus the molecular mechanism remains to be elucidated.

Dehydration stress leads to the reduction of a cell volume and the destruction of cell structures, causing cells severe mechanical stress. To protect cells from these deformative forces, cytoskeletons like intermediate filaments (IFs) are generally principal players in counteracting mechanical stress in ordinary animal cells [19,20]. Tardigrades have actin filaments and microtubules, but largely lack cytoplasmic IFs, except a tardigrade-unique IF protein called cytotardin [21]. Cytotardin is not homologous to any cytoplasmic IFs in other animals and rather derives from the nuclear filament protein lamin. Cytotardin does not localize to the nucleus because it lacks a nuclear localization signal, and instead forms belt-like filaments beneath the plasma membrane encircling epithelial cells, suggesting its contribution to the mechanical strengthening of epithelial tissues. In tardigrades, no IFs are known to form scaffold-like filamentous networks in the cytosol, which is thought to effectively counteract the deformative forces in many other animal cells [22,23].

In this study, we postulated the presence of tolerance proteins that form protective condensates in a stress-dependent manner, and comprehensively searched for such proteins in tardigrade lysate. Among more than 300 identified proteins that we collectively dubbed "dehydration-induced reversibly condensing proteins (DRPs)", we unexpectedly rediscovered CAHS proteins as highly-enriched and major components of DRPs. Further analysis revealed that in response to stress, CAHS reversibly forms many cytoskeleton-like filaments in cultured cells and also exhibits reversible gelation *in vitro*, which increases the mechanical strength of cell-like microdroplets. We also examined the structural basis required for filament formation by deletion and point mutation analyses. By studying the generated filament-defective mutants, we confirmed that the filament-forming ability is the basis for the gel transition of CAHS proteins. On the basis of these results, we propose a new tolerance model in which CAHS proteins act as a kind of cytoskeleton that reversibly forms intracellular filamentous networks in response to dehydration and induces gel transition that increases mechanical strength of cells and contributes to the desiccation tolerance of tardigrades.

Results

Dehydration-dependent reversibly condensing proteins (DRPs) are identified from *Ramazzottius varieornatus*

We designed the experimental scheme shown in Fig 1A to identify tardigrade proteins that form condensates in response to dehydration-like stress in a reversible manner. We began with the lysate of the desiccation-tolerant tardigrade species *R. varieornatus*, because this species constitutively expresses the tolerance proteins and its genome sequence is available [15]. First, we added trifluoroethanol (TFE) to a soluble fraction of *R. varieornatus* lysate to induce condensation in a dehydration-like state. TFE is a desolvating reagent that induces dehydration-like conformational changes in several desiccation-tolerance proteins, such as LEA and CAHS proteins [16,24,25]. The TFE-condensed proteins were collected as precipitates and resolubilized with TFE-free PBS to mimic rehydration. Without TFE treatment, no proteins were detected in the resolubilized fraction. In contrast, treatment with a higher concentration of TFE increased the number of proteins detected in the resolubilized fraction (Figs 1B and S1). As treatment with 20% and 30% TFE had similar effects, we considered 20% TFE to be an adequate stress condition for this screening (Fig S1). When treated with TFE at 20% or higher, many proteins, especially those with a high molecular weight, were detected in the irreversibly precipitated fraction, indicating that only the selected proteins were retrieved in the resolubilized fraction.

We identified 336 proteins in the resolubilized fraction (20% TFE) by liquid chromatography-tandem mass spectrometry (LC-MS/MS), and collectively termed these proteins “dehydration-dependent reversibly condensing proteins (DRPs)”. Reversible condensation is a characteristic property expected for unstructured proteins. To evaluate whether unstructured proteins are enriched in DRPs, we calculated the unstructured score of each protein by IUPred2A and compared the score distribution between DRPs and all tardigrade proteins. As expected, DRPs contained a significantly higher proportion of unstructured proteins ($p < 2.2e\text{-}16$, Wilcoxon rank sum test; Fig 1C). We assigned *Drosophila melanogaster* orthologs for tardigrade proteins and performed enrichment analysis of PANTHER Protein class or Gene Ontology term in DRPs. The results revealed that ribosomal proteins

and actin-related cytoskeletal proteins were well concentrated in DRPs (Figs 1D and S2). Among DRPs, however, 105 (31%) proteins had no apparent fly orthologs and DRPs contain many tardigrade-unique proteins (21%) including known tolerance proteins like CAHS proteins. Therefore, we expanded the enrichment analyses to the previously annotated tardigrade tolerance protein families that contain more than 5 members [15], and revealed the significant enrichment of CAHS, LEA, HSP20, HSP70 and peroxiredoxin families in DRPs ($p < 0.01$, chi-square test; Fig 1E), suggesting that our new screening scheme concentrates desiccation-tolerance related proteins to the resolubilized fraction. To evaluate this possibility further, we classified DRPs into 3 groups: stress-upregulated groups, stress-downregulated groups, and others. *R. varieornatus* is one of the toughest tardigrade species that constitutively expresses stress-related genes [15]. Thus, we utilized gene expression data of 2 closely related tardigrades, *Hypsibius exemplaris* and *Paramacrobiotus* sp. TYO, both of which exhibit strong up-regulation of tolerance gene expression upon desiccation [11,26]. Of 336 DRPs, 316 proteins had orthologs in both species and 74 genes were upregulated during dehydration (Fig 1F). Statistical analysis indicated that the up-regulated proteins were significantly enriched in DRPs compared with the tardigrade proteome ($p = 1.36e-33$, chi-square test). In addition, the up-regulated proteins also exhibited a much higher unstructured score (Fig 1G), suggesting that tolerance-related unstructured proteins were well concentrated in the resolubilized fraction in our scheme. Because CAHS proteins were highly enriched in the DRPs (Fig 1E), and also 3 major bands in the resolubilized fraction were separately identified as CAHS12, CAHS3, and CAHS8 (Figs 1B and S3), we focused on these 3 CAHS proteins for further analyses.

CAHS3, CAHS8, and CAHS12 reversibly assemble into filaments or granules in human cultured cells depending on hyperosmotic stress

To visualize the stress-dependent condensation of 3 CAHS proteins, GFP-fused CAHS3, CAHS8, and CAHS12 proteins were separately expressed in human cultured HEp-2 cells and the distribution changes of these fusion proteins upon exposure to a hyperosmotic stress, which induces water efflux like dehydration stress [27], was examined. In an unstressed condition, CAHS3-GFP broadly

distributed in the cytosol, whereas CAHS8-GFP and CAHS12-GFP distributed broadly in both the cytosol and the nucleus with CAHS12-GFP showing a slight preference for the nucleus (Fig 2A). When exposed to hyperosmotic medium supplemented with 0.4 M trehalose, CAHS3-GFP condensed and formed a filamentous network in the cytosol (Fig 2A and 2B). Similar filament formation was observed when CAHS3 alone was expressed without GFP (Fig S4), suggesting that filament formation is an intrinsic feature of CAHS3 protein rather than artifact of fusion with GFP. CAHS12-GFP also formed filaments in the cytosol and more prominently in the nucleus in a majority of cells, though granule-like condensates were also observed in the nucleus of approximately 34% of the cells (Figs 2B and S5). CAHS8-GFP predominantly formed granule-like condensates especially in the nucleus, but filaments were also observed in the cytosol in a small population (~ 3%) of the cells. Similar distribution changes were observed even when GFP was fused to the opposite site in CAHS proteins (Fig S6), while GFP alone did not exhibit such drastic changes. When hyperosmotic stress was removed by replacing with isosmotic medium, all CAHS condensates, both filaments and granules, rapidly dispersed (Fig 2A and 2B). Hyperosmotic stress by other supplemented osmolytes, such as 0.2 M NaCl or 0.4 M sorbitol, which have an equivalent osmolarity to 0.4 M trehalose, induces similar filament or granule formation, suggesting that the condensations of CAHS proteins are induced by hyperosmotic stress itself rather than specific effects of each osmolyte (Fig S7). Similar reversible condensations of CAHS proteins were also observed when expressed in *Drosophila* cultured S2 cells (Fig S8), indicating that the stress-dependent filament/granule condensations are intrinsic features of CAHS proteins commonly observed in animal cells of taxonomically distant species.

Granule-like condensates of CAHS8 resemble droplet structures formed by intrinsically disordered proteins via liquid-liquid phase separation. To test this possibility, we examined the effect of 1,6-hexanediol, a disruption reagent of liquid-like condensates. After treatment with 5% 1,6-hexanediol for 30 min, the well-known droplet-forming protein FUS effectively dispersed, while several CAHS8 granules in the nucleus also dispersed but much less effectively than FUS protein granules (Fig 2C), suggesting that CAHS8 granules were partly liquid-like, i.e., between liquid and

198 solid states. In contrast, the filament structures of CAHS3 or CAHS12 were not affected by the
199 hexanediol treatment, suggesting that CAHS3 and CAHS12 filaments were in a static solid-like state.
200 To further assess the staticity of CAHS filaments, we performed fluorescence recovery after
201 photobleaching (FRAP) analysis on CAHS3-GFP both before and after exposure to hyperosmotic
202 stress. In unstressed cultured cells, CAHS3-GFP was broadly distributed in the cytosol and the
203 bleached fluorescence was rapidly recovered (Fig 2D), indicating their high mobility nature. In
204 contrast, under hyperosmotic stress, CAHS3-GFP filaments exhibited almost no fluorescence recovery
205 after bleaching (Fig 2E). These results demonstrated that CAHS3 molecules freely disperse in an
206 unstressed condition, but upon the exposure to hyperosmotic stress, CAHS3 molecules are firmly
207 integrated into a filament and lose their mobility.
208 To elucidate the process of filament formation and deformation in more detail, we captured time-
209 lapse images of cells expressing CAHS3-GFP while changing the stress conditions by high-speed
210 super-resolution microscopy. Approximately 2.5 min after the medium was changed to a hyperosmotic
211 condition by a perfusion device, CAHS3-GFP began to condense simultaneously at many sites in the
212 cells and rapidly formed fibril structures. The fibrils then further extended in a few dozen seconds (Fig
213 2F and Movie S1). When the hyperosmotic stress was removed by changing to an isosmotic medium,
214 CAHS3 filaments simultaneously began to loosen and gradually dispersed in approximately 6 min
215 (Fig 2G and Movie S2). The initial condensation of CAHS3 and the granule formation of CAHS8
216 likely occurred via phase-separation, which frequently leads to co-condensation of multiple proteins,
217 especially those containing similar motifs [28]. CAHS proteins share several conserved motifs and
218 could thus cooperatively form the same condensates. To examine this, we co-expressed pairs of the 3
219 CAHS proteins labeled with different fluorescent proteins in human cells. Under hyperosmotic stress,
220 CAHS3 filaments did not co-localize with CAHS8 granules or CAHS12 filaments (Fig 3), suggesting
221 no interaction between them. In contrast, CAHS8 largely co-localized with CAHS12 filaments
222 throughout the cell, suggesting that the granule-forming CAHS8 cooperatively forms the filament
223 structure with other CAHS proteins such as CAHS12.
224

Filament formation of CAHS3 or CAHS12 is independent of other cytoskeletons

Filamentous networks formed by CAHS3 or CAHS12 proteins resembled cytoskeletal structures. To examine whether the CAHS proteins formed filaments exclusively or cooperatively with other cytoskeletal structures or organelles, we co-visualized major cytoskeletons or organelles by expressing cytoskeleton/organelle marker proteins tagged with fluorescent proteins and then compared those with the distribution of CAHS-GFP filaments in human cells. As shown in Figs 4A–4C and S9A–S9D, the CAHS3-GFP filaments and CAHS12-GFP filaments did not overlap with any examined cytoskeleton and organelles, such as microtubules, various intermediate filaments, mitochondria, and endoplasmic reticulum, except for a slight co-localization with actin filaments. Because GFP alone also exhibited partial co-localization with actin filaments under a hyperosmotic condition (Fig 4D), we assumed that the GFP-moiety is responsible for this slight co-localization between CAHS-GFP and actin filaments. To clarify the independence of CAHS filament formation from actin filaments, we treated the cells with an actin polymerization inhibitor, cytochalasin B. As a result, actin-filaments were significantly disrupted, but CAHS filaments were not affected (Fig 4E), suggesting that filament formation of both CAHS3 and CAHS12 is independent from actin filaments. CAHS8-GFP unexpectedly co-localized with an intermediate filament, vimentin (Fig S9B), in addition to actin filaments. CAHS8 could interact with vimentin filaments under hyperosmotic stress in human cells, though no vimentin genes were found in the tardigrade genome [21].

C-terminal regions are necessary and sufficient for filament-formation by both CAHS3 and CAHS12

To reveal the structural basis of CAHS filament formation, we first searched and found 10 conserved motifs by comparing 40 CAHS proteins of 3 tardigrade species, *R. varieornatus*, *H. exemplaris*, and *Paramacrobiotus* sp. TYO (Figs S10 and S11). In particular, we found that 2 C-terminal motifs (CR1 and CR2) are highly conserved in all CAHS family members except 1 CAHS protein of *H. exemplaris* (Figs 5A and S10). To determine the region responsible for filament formation, we generated a series of truncated mutant proteins of CAHS3 or CAHS12 either N-terminally or C-terminally, and examined

252 their filament formation in human cultured cells under a hyperosmotic stress (Fig 5B and 5C). In
253 CAHS3, N-terminal deletion to motif 3 or C-terminal deletion to CR2 drastically impaired filament
254 formation and instead granule formation was frequently observed in the cytosol (Figs 5B and S12).
255 Accordingly, we designed a truncated mutant consisting of the minimum required region from motif
256 3 to CR2 (motif 3-motif H1-CR1-CR2), and revealed that this region is sufficient for the filament
257 formation by CAHS3 protein (Fig 5B). Similarly, in CAHS12 protein, the region consisting of CR1,
258 CR2, and the 2 preceding motifs (motif H2-motif H3-CR1-CR2) was shown to be necessary and
259 sufficient for the filament formation (Fig 5C). These results indicated that 2 highly conserved motifs
260 (CR1 and CR2) and 2 preceding motifs (65~85 residues) play an essential role in the filament-
261 formation of both CAHS3 and CAHS12 proteins.
262
263 **Helix-disrupting mutations in CR impair filament formation of CAHS3 and CAHS12**
264 In the regions responsible for the filament formation of both CAHS3 and CAHS12 proteins, extensive
265 helix and putative coiled-coil structures were predicted by the secondary structure prediction tool,
266 JPred4 and COILS (Figs 6 and S13). The coiled-coil structure is the key structural basis for the
267 polymerization of intermediate filaments [29]. To test whether these predicted secondary structures
268 are important for filament formation, we generated 2 mutants for each CAHS3 and CAHS12 by
269 substituting leucine with proline, which are predicted to disrupt the helical and coiled-coil structures
270 of CR1 or CR2, respectively (Fig 6) [30]. As expected, all coiled-coil disruption mutants failed to form
271 filaments and instead formed granules (Figs 6 and S14). The double mutation (CAHS3-L207P-L236P)
272 further suppressed filaments formation and even reduced granule formation (Figs 6A and S16). These
273 results suggested that the secondary structures of both CR1 and CR2 are an important basis for the
274 filament formation by CAHS3 and CAHS12 proteins.
275
276 ***In vitro* reversible gel transition of CAHS proteins depending on desolvating reagent and salt**
277 To examine whether CAHS proteins alone are sufficient to form filaments, we performed *in vitro*
278 experiments using purified CAHS3-GFP proteins. Under an unstressed condition, the uniform

279 distribution of CAHS3-GFP proteins was observed under a confocal microscope (Fig 7A). When the
280 desolvating reagent TFE was added to induce a dehydration-like conformational change as in our
281 initial screening, CAHS3-GFP immediately condensed and formed mesh-like fibril networks after 1
282 min. This result indicated that CAHS3 proteins alone can sense the changes in the condition and form
283 filaments without the assistance of other proteins.

284 When TFE was added to the solution containing a higher concentration of purified CAHS3
285 protein (final 4 mg/mL; Fig S17), the protein solution immediately became turbid, and the solution
286 was solidified into a gel-like state (Fig 7B, upper panels). When the CAHS3 gel in the tube was spread
287 onto parafilm, the CAHS3 gel spontaneously liquefied within approximately 10 min. We speculated
288 that volatilization of TFE relieved the desolvating stress, thereby making the CAHS3 gel resoluble.
289 Consistently, washing with TFE-free PBS also redissolved the gelated CAHS3 (Fig S18). While the
290 control protein BSA was not solidified in the same condition (Fig S19), CAHS8 and CAHS12
291 exhibited a similar TFE-dependent reversible gel-transition like CAHS3, but the gel of CAHS8 was
292 much smaller than those of other CAHS proteins (Fig 7B, middle and lower panels), suggesting
293 differences in the propensity for gelation among CAHS proteins. We also examined whether other
294 stressors that could emerge during dehydration induce CAHS gelation and revealed that an increased
295 concentration of salt (2 M NaCl) also induced the gel-transition of CAHS3 proteins (Fig 7C), while a
296 molecular crowding agent (20% polyethylene glycol) caused turbidity, but no gelation (Fig 7D). The
297 salt-induced gel persisted even after exposure to air on parafilm, possibly because salt cannot
298 evaporate (Fig. 7C). The granule-forming CAHS8 only formed a very small gel *in vitro*, implying a
299 possible relationship between the filament-forming ability in cells and the gel-forming ability *in vitro*.
300 This notion was supported by the fact that the filament-deficient CAHS3-L207P mutant protein failed
301 to form the gel *in vitro* (Fig 7E). In contrast, minimum CAHS3 protein possessing the filament-forming
302 ability (CAHS3-min) successfully formed the gel *in vitro* upon the addition of TFE and this transition
303 was reversible as in full-length CAHS3 (Fig 7 F), suggesting that filament-forming ability underlies
304 the gel transition of CAHS proteins *in vitro*.
305

306 **Gelation of CAHS3 improves mechanical strength of a cell-like microdroplet**

307 To reveal what the gelation of CAHS proteins provides, we evaluated the effects of CAHS gelation on
308 the mechanical properties of cells using cell-like microdroplets covered with a lipid layer. The
309 elasticity of the microdroplets was examined by measuring the elongation length in a micropipette
310 while aspirating with a certain pressure. Microdroplets containing uniformly distributed CAHS3-GFP
311 exhibited continuous elongation exceeding 50 μm under very small pressure (<< 0.5 kPa), indicating
312 that they were not elastic and in a liquid phase (Fig 8). On the other hand, the addition of salt induced
313 the filament formation by CAHS3-GFP and the corresponding microdroplets exhibited significant
314 elasticity (Young's modulus ~2.0 kPa in average), indicating that the CAHS3-GFP droplets gelated
315 and then physically hardened. Microdroplets containing GFP alone were not elastic regardless of the
316 addition of salt (Fig 8B and 8C).
317
318

Discussion

Our study provides evidence that CAHS proteins reversibly condense in a stress-dependent manner and form a cytoskeleton-like filamentous network in animal cells or undergo gel-transition *in vitro*, which increases the mechanical strength of cell-like microdroplets (Figs 2A, 7B and 8). CAHS proteins were thought to act as a vitrifying agent like trehalose during dehydration based on the shift in differential scanning calorimetry (DSC) [17], but this hypothesis was recently counter-argued with data demonstrating that the shift in DSC can be explained by water retention of CAHS proteins [18]. Because hydrogel generally has high water retention properties, our observation of gel-transition by CAHS proteins supports the water retention in the counterargument rather than vitrification. *In vitro* gel transition was observed when using a relatively high concentration (~ 4 mg/mL) of CAHS solution (Fig 7B), and filament-defective CAHS mutants failed in transition to gel (Fig 7E), suggesting that a dense filament formation is the structural basis for the gel transition of CAHS proteins. The tolerant tardigrade *R. varieornatus* expresses a remarkable amount of CAHS family genes (total tpm ~11,000) [15,16], and the cell volume reduction during dehydration leads to a significant increase in both the protein concentration and ion strength that might be one of the gel-inducing factors as shown in Fig 7C, suggesting that the intracellularly abundant CAHS proteins undergo gel-transition in tardigrade cells and provide mechanical stabilization of cell integrity during dehydration (Fig 8), which could partly account for the exceptional stability of dehydrated tardigrades. The sol-gel transition of CAHS proteins was highly reversible and stress-dependent, and FRAP analysis revealed that CAHS proteins were immobile only when filaments formed under a stress condition. Therefore, we suppose that CAHS proteins are freely dispersed in a hydrated condition to minimize interference with other biological processes, whereas in a dehydrated condition, CAHS proteins form an intracellular filamentous network and elastic hydrogel to provide mechanical stabilization of cell integrity.

Although CAHS proteins exhibit no sequence similarity with any other cytoskeletal proteins, CAHS proteins formed cytoskeleton-like filamentous networks independently from the other cytoskeleton under a hyperosmotic stress (Figs 4 and S9). Hence, we propose CAHS proteins as a novel cytoskeletal protein family with stress-dependence and gel-forming ability. Although no known

346 motifs are found in the primary sequence of CAHS proteins, the C-terminal region including the highly
347 conserved CR1 and CR2 motifs was essential and sufficient for the filament formation (Fig 5). This
348 region was mostly predicted as helical and to form a coiled-coil structure (Figs 6 and S13). This
349 prediction was also supported by the previous circular dichroism analysis demonstrating that CAHS1
350 protein, another member of the CAHS family, becomes alpha-helical upon desolvating stress from the
351 unstructured state in a hydrated condition [16]. The severe impairments in the filament formation by
352 proline substitutions in either the CR1 or CR2 region (Fig 6) also indicate that the secondary structure
353 of CR1 and CR2 plays important roles in CAHS filament formation. Some intrinsically disordered
354 proteins are reported to form a gel-like state in granule condensates via promiscuous binding through
355 multivalent interaction sites [31], but in CAHS3 and CAHS12, single amino acid substitution is
356 enough to disrupt both filament formation and gel transition, suggesting that the mechanism of
357 filament/gel formation of CAHS proteins is likely not due to multivalent interactions, but rather to
358 polymerization based on the secondary structure. The prediction of 3-dimentional structures by
359 AlphaFold2 [32,33] suggested that CAHS3-min proteins form a helix in the CR1+CR2 region with
360 high confidence (pLDDT = 70~90) and 2 CAHS3-min proteins form an anti-parallel dimer with the
361 juxtaposition of each helical region where the charge and hydrophobicity distribution is consistent
362 with the stabilization of 2 helix interactions (S20). The anti-parallel helical dimer is a key structural
363 basis for the fiber formation of intermediate filament proteins, e.g., lamin monomers dimerize by
364 forming coiled-coils bind via hydrophobic interaction [29]. Similar to intermediate filaments, CAHS
365 proteins might also be assembled to fibers via a coiled-coil structure.

366 In contrast to filament-forming CAHS3 and CAHS12, CAHS8 alone formed granule-like
367 condensates in both human and insect cells under a hyperosmotic condition (Figs 2A and S8). Stress-
368 dependent granule condensation by CAHS8 resembled the stress-granule formation in mammalian
369 cells that occurs through phase separation to create protective membrane-less compartments against
370 stress [34,35]. A recent study revealed that another desiccation tolerance protein, AfrLEA6, which is
371 a group 6 LEA protein of *Artemia franciscana*, also undergoes phase separation to form granules in
372 insect cells [14] and protects enzyme activity from desiccation stress *in vitro* [36]. Like stress-granules

and AfrLEA6 granules, CAHS8 granules exhibited certain sensitivity against 1,6-hexanediol treatment (Fig 2C). CAHS8 might exert similar protective functions via granule condensation under stress conditions. Alternatively, in cells co-expressing CAHS8 and CAHS12, as shown in Fig 3, CAHS8 contributes to filament formation with CAHS12 in tardigrades.

Our isolation scheme (Fig 1A) successfully identified CAHS proteins that reversibly condensed to filaments or granules in a stress-dependent manner from anhydrobiotic tardigrades. Although CAHS proteins are conserved only in tardigrades, proteins with similar properties might be present in other desiccation-tolerant organisms and may contribute to stress resistance. Our isolation scheme of DRPs may provide a general and potent method to identify unstructured proteins that undergo reversible condensation to filaments or granules in a stress-dependent manner from various organisms. CAHS proteins were originally identified by searching for heat-soluble proteins to identify anhydrobiotic protectants in tardigrades [16]. Later, using a similar method, many heat-soluble proteins were identified from humans and flies, dubbed Hero proteins [37], that exhibit no sequence similarity with CAHS proteins but provide stabilization of other proteins such as CAHS or LEA proteins do. Similarly, future DRPome analysis may lead to the identification of protective phase-separating proteins even in non-anhydrobiotic organisms.

In the present study, we established a new method to comprehensively identify proteins that are reversibly condensed in response to desolvating stress and found 336 such proteins from desiccation-tolerant tardigrades. The major components, CAHS3 and CAHS12, were shown to form cytoskeleton-like filaments and elastic hydrogel in a stress-dependent manner. We propose that these CAHS proteins function as novel stress-dependent and gel-forming cytoskeletal proteins that provide mechanical strength to stabilize cellular integrity during stress. Our data suggested a novel desiccation tolerance mechanism based on filament/gel formation. The isolation scheme established in this study opens the way to identifying such novel stress-dependent cytoskeletal proteins from various organisms.

Materials and Methods

Animals

We used the previously established YOKOZUNA-1 strain of the desiccation-tolerant tardigrade *R. varieornatus* reared on water-layered agar plate by feeding alga *Chlorella vulgaris* (Recenttec K. K., Japan) at 22°C as described previously [38].

Identification of dehydration-dependent reversibly condensing proteins

Prior to protein extraction, tardigrades were starved for 1 day to eliminate digestive food. Approximately 400 *R. varieornatus* were collected and extensively washed with sterilized Milli-Q water to remove contaminants. Tardigrades were rinsed with lysis buffer, phosphate-buffered saline (PBS; 137 mM NaCl, 2.7 mM KCl, 10 mM Na_2HPO_4, 1.76 mM KH_2PO_4, pH 7.4) containing cOmplete protease inhibitors (Roche), and transferred to a 1.7 mL tube. Tardigrades were homogenized in 20 µL lysis buffer using a plastic pestle on ice. The pestle was rinsed with an additional 20 µL of lysis buffer collected in the same tube. After centrifugation at 16,000 × g for 20 min at 4°C, the supernatant was recovered as a soluble protein extract. To mimic dehydration stress, the desolvating agent, trifluoroethanol (TFE), was added (final concentration 10%, 20%, or 30%) and the mixture was incubated on ice for 1 h to allow complete induction of condensation. After centrifugation at 16,000 × g for 20 min, the supernatant was removed as a TFE-soluble fraction and the remaining precipitate was washed twice by lysis buffer containing TFE at the same concentration. The washed precipitate was resuspended in lysis buffer without TFE, and incubated at room temperature for 30 min to facilitate resolubilization. After centrifugation at 16,000 × g at 4°C, the supernatant was recovered as a resolubilized fraction. The fractions were analyzed by SDS-PAGE and proteins were visualized using a Silver Stain MS Kit (Fujifilm). Three selected bands were excised and separately subjected to mass spectrometry. Comprehensive identification of DRPs was achieved by shot-gun proteomics of the resolubilized fraction. Briefly, proteins in gel slices or in the fraction were digested with trypsin and fragmented peptides were analyzed by nano LC-MS/MS. Proteins were identified using MASCOT software (Matrix Science).

426

427 ***In silico* structure predictions**

428 The unstructured score of the proteins was calculated by IUPred2A [39]. IUPred2A produces the score
429 for each amino acid position in a protein, and an average value was used as a score for each protein.
430 A *de novo* protein sequence motif search in CAHS protein families was performed by the motif
431 discovery tool, MEME version 5.0.4 [40] (https://meme-suite.org/meme/tools/meme). The parameters
432 were as follows: (occurrence per sequence = 0 or 1; the maximum number to be found = 10; the motif
433 width = 6 to 50). The secondary structures of CAHS3, CAHS8, and CAHS12 proteins were predicted
434 by JPred4 [41] (https://www.compbio.dundee.ac.uk/jpred/). The coiled-coil regions of CAHS3 and
435 CAHS12 were predicted by COILS [42] (https://embnet.vital-it.ch/software/COILS_form.html). The
436 3-dimensional structure prediction of the CAHS-min protein homo-dimer was performed by
437 Alphafold2 [33]
438 (https://colab.research.google.com/github/sokrypton/ColabFold/blob/main/AlphaFold2_complexes.i
439 pynb). The 3-dimensional structures were visualized with UCSF ChimeraX v.1.2 [43].

440

441 **Enrichment analysis**

442 To utilize well-annotated information in the model organism *Drosophila melanogaster*, we assigned a
443 *D. melanogaster* ortholog for each *R. verieornatus* protein by a reciprocal BLAST search. We assigned
444 231 fly orthologs for 336 DRPs and 7,361 fly orthologs for all 19,521 *R. varieornatus* proteins. Using
445 the assigned fly orthologs, we performed enrichment analyses with PANTHER Overrepresentation
446 Test [44] (PANTHER Protein Class version 16.0, Fisher's test; http://pantherdb.org/) and Metascape
447 [45] (GO Cellular Components; https://metascape.org/). The list of fly orthologs for all *R. varieornatus*
448 proteins was used as a reference in the enrichment analyses.

449 Among tardigrade stress-related proteins described previously [15], 7 protein families containing
450 more than 5 members were selected for the enrichment analysis. Enrichment of each family in DRPs
451 was statistically examined by Fisher's exact test using R. Enrichment of up-regulated genes was
452 similarly examined except a chi-square test was used.

453

454 **Differential gene expression analysis**

455 Transcriptome data at a hydrated state and a dehydrated state were retrieved from the public database
456 (DRR144971-DRR144973 and DRR144978-DRR144980 for *Paramacrobiotus* sp. TYO;
457 SRR5218239-SRR5218241 and SRR5218242-SRR5218244 for *Hypsibius exemplaris*, respectively).

458 The genome sequence of *H. exemplaris* v3.0 was retrieved from http://www. tardigrades.org.
459 RNA-seq reads were mapped to the genome sequence using HISAT2 v.2.1.0 [46]. Read counts for
460 each gene region were quantified by featureCounts in SubRead package v.1.6.3 [47] and statistically
461 compared by R package DESeq2 [48]. The genes with FDR < 0.01 were considered as differentially
462 expressed genes. Orthologous gene relationships were determined by reciprocal BLAST searches
463 among 3 tardigrade species.

464

465 **Cell lines**

466 We obtained HEp-2 cells (RCB1889) from RIKEN BioResource Center (BRC). The identity of the
467 cell line was validated by short tandem repeat profiling and the cell line was negative for mycoplasma
468 contamination (RIKEN BRC). The cell was maintained in minimum essential medium (Nacalai
469 Tesque) containing 10% fetal bovine serum (FBS, Cosmo Bio or BioWest) at 37°C, 5% CO_2.
470 *Drosophila* S2 cells (Gibco) were cultured at 28°C in Schneider's *Drosophila* Medium (Gibco)
471 supplemented with 10% heat-inactivated FBS (BioWest) and penicillin-streptomycin mixed solution
472 (Nacalai Tesque).

473

474 **Plasmids**

475 CAHS3, CAHS8, and CAHS12 coding sequences were amplified from the corresponding EST clones
476 of *R. varieornatus* [15] and inserted into pAcGFP1-N1 or pAcGFP1-C1 (Clontech) with $(GGGGS)_3$
477 linker using In-Fusion HD Cloning Kit (Takara). Plasmids to express CAHS deletion mutants
478 (CAHS3ΔCtail, CAHS3ΔCR2-C, CAHS3ΔN-M2, CAHS3ΔN-M3, CAHS3-min, CAHS12ΔCtail,
479 CAHS12ΔCR2-C, CAHS12ΔN-M1, CAHS12ΔN-H2, and CAHS12-min) or leucine-to-proline

480 substitution mutants (CAHS3-L207P, CAHS3-L236P, CAHS3-L207P-L236P, CAHS12-L204P and
481 CAHS12-L241P) were generated by inverse PCR and ligation, or PCR-based site directed mutagenesis.
482 The CAHS3/8/12-mScarlet-I expression vector was generated from CAHS3/8/12-GFP expression
483 vector by replacing AcGFP1 coding sequences with *mScarlet-I* sequence fragments [49] synthesized
484 artificially (IDT). Expression constructs for various cytoskeleton or organelle marker proteins were
485 obtained from Addgene (Table S1). For bacterial expression of His-tagged CAHS proteins, *CAHS3*,
486 *CAHS8* or *CAHS12* coding sequences were amplified and inserted into pEThT vectors [16], and
487 *CAHS3-GFP* was similarly inserted into a pCold-I vector (Takara). For expression in *Drosophila* cells,
488 codon-optimized *CAHS3*, *CAHS8*, *CAHS12*, and *AcGFP1* DNA fragments were synthesized (Gene
489 Universal) and inserted into pAc5.1/V5-His A vector (Invitrogen). The FUS-Venus plasmid was a kind
490 gift from Dr. Tetsuro Hirose.
491
492 **Live cell imaging under hyperosmosis**
493 HEp-2 cells were transiently transfected with an expression vector of fluorescently labeled proteins
494 using Lipofectamine LTX & Plus Reagent (Invitrogen) for 48 h before stress exposure. Prior to
495 microscopy, the medium was replaced with Hanks' Balanced Salt Solution (HBSS) without the
496 dications and phenol red. For exposure to hyperosmotic stress, the buffer was replaced with HBSS
497 containing 0.4 M trehalose. The cells were stained with Hoechst 33342 (5 µg/mL, Lonza) to visualize
498 nuclear DNA. Fluorescent signals were observed using a confocal microscope LSM710 (Carl Zeiss).
499 The number of cells for each CAHS distribution pattern, such as dispersed, granules or filaments, were
500 counted by 2 independent investigators and averaged counts were used. For time-lapse imaging in 3-
501 dimensional space, we used the LSM-980 with Airyscan to perform super-resolution imaging. From
502 the z-stack images, we generated orthogonal projections using ZEN 2.6 software. In time-lapse
503 imaging experiments, a perfusion system KSX-Type1 (Tokai Hit) was used to replace the buffer. To
504 visualize actin filaments by chemical staining, HEp-2 cells were treated with silicon-rhodamine dye
505 probing actin (SiR-actin, Spirochrome) in HBSS containing the drug efflux inhibitor verapamil (10
506 µM, Tokyo Chemical Industry) for 2 h. For actin polymerization inhibition experiments, cells were

507 treated with cytochalasin B (5 μM, Nacalai Tesque) for 60 min. Cells were then observed by a confocal
508 microscope LSM-710 (Carl Zeiss).
509
510 **Fluorescence recovery after photobleaching (FRAP) analysis**
511 HEp-2 cells were transiently transfected with the expression construct of CAHS3-GFP. The transfected
512 cells were then exposed to isosmotic HBSS or hyperosmotic buffer, HBSS containing 0.4 M trehalose,
513 to analyze the mobility of CAHS3-GFP in the dispersed or filament state, respectively. FRAP
514 experiments were performed at room temperature using a confocal fluorescence microscope (FV1200,
515 Olympus). A spot approximately 0.77 μm in diameter was photobleached at 100% laser power
516 (wavelength 473 nm), and the fluorescence recovery curves were analyzed using the Diffusion
517 Measurement Package software (Olympus). The fluorescence intensity was normalized by the initial
518 intensity before photobleaching.
519
520 **Sensitivity to 1,6-hexanediol treatment**
521 HEp-2 cells were transfected with expression vectors of CAHS3/8/12-AcGFP1 or FUS-Venus. After
522 48 h, cells were exposed on minimum essential medium supplemented with 0.4 M trehalose and 10%
523 FBS for 1 h to induce the formation of granules or filaments. FUS protein was used as a control as it
524 is known to be incorporated into liquid droplets under hyperosmosis [50]. After the addition of a liquid
525 droplet disruptor, 1,6-hexanediol (final 5%), fluorescent images were captured at 0 and 30 min later
526 by a confocal microscope LSM710 (Carl Zeiss). The fluorescence intensity was measured by Fiji and
527 normalized to the initial fluorescence intensity of the granules or filaments.
528
529 **Immunofluorescence**
530 HEp-2 cells expressing CAHS3 or CAHS3 mutants were exposed to HBSS containing 0.4 M trehalose
531 for 60 min to induce filament-formation. The cells were then fixed in methanol at -30°C for 3 min and
532 washed 3 times with PBS containing 0.1% Tween 20 (PBS-T). The cells were blocked with 2% normal
533 goat serum (Abcam) for 1 h at room temperature and then reacted with 1/200 diluted antiserum against

CAHS3 in 2% normal goat serum for 1 h at room temperature or 16 h at 4°C. The cells were washed 3 times with PBS-T, and then reacted with 1/1,000 diluted Alexa Fluor546 goat anti-guinea pig secondary antibody (Invitrogen) and 1 μg/mL DAPI in 2% normal goat serum for 1 h at room temperature. Fluorescent signals were observed using a confocal microscope LSM710 (Carl Zeiss).

Protein preparation

Recombinant proteins were expressed as N-terminally 6×His-tagged proteins in *Escherichia coli* BL21(DE3) strains. CAHS3, CAHS8, and CAHS12 proteins were expressed using pET system (Novagen) essentially as described previously [16]. CAHS3-GFP and AcGFP1 were expressed using a cold shock expression system (Takara) essentially as described previously [51]. Bacterial pellets were lysed in PBS containing cOmplete EDTA-free protease inhibitors (Roche) by sonication. For CAHS3, CAHS8 and CAHS12, the supernatant was heated at 99°C for 15 min to retrieve heat-soluble CAHS proteins in a soluble fraction as described previously [16]. From the soluble fraction, His-tagged proteins were purified with Ni-NTA His-Bind Superflow (Novagen) and dialyzed against PBS using a Pur-A-Lyzer™ Midi Dialysis Kit (Merck).

***In vitro* polymerization of CAHS3-GFP proteins**

Purified CAHS3-GFP or AcGFP1 protein solution in PBS (~ 40 μM) was directly dropped on cover glass (MATSUNAMI), and fluorescent images were captured by a confocal microscope LSM710 (Carl Zeiss). To the induce polymerization of CAHS3, an equal amount of PBS containing TFE (final 20%) was added, and time-lapse images were captured every 5 s.

***In vitro* gelation**

Purified recombinant CAHS protein solution (5 mg/mL) was placed in a 0.2-mL tube. Inducing reagents such as TFE (final 20%), polyethylene glycol (final 30%), or NaCl (final 2 M) were added to the protein solution and incubated at room temperature for 10 min. Then, the tube contents were spread

out on parafilm to check if it had solidified into a gel-like state or remained in a liquid state. Photos were obtained by a digital camera with a short focal length (Olympus TG-6).

Preparation of cell-like microdroplets

Cell-like microdroplets coated with a lipid layer of phosphoethanolamine (Nacalai Tesque) were prepared in an oil phase. First, dry films of the lipids were formed at the bottom of a glass tube. Mineral oil (Nacalai Tesque) was then added to the lipid films followed by 90 min of sonication. The final concentration of the lipid/oil solution was approximately 1 mM. Next, 10 vol % of the protein solution (40 μM GFP-labeled CAHS3 or 40 μM GFP) was added to the lipid/oil solution at ~25°C. After emulsification via pipetting, the ~40 μL sample containing the microdroplets was placed on a glass-bottom dish. To condense the proteins inside the droplets upon dehydration, we added 40 μL salted oil. Mechanical measurements were performed 90 min after the droplet volume was approximately halved. For fluorescent imaging, 21 μM CAHS3-GFP and 171 μM CAHS3 were mixed and used.

Measurement of the elasticity of droplets by micropipette aspiration

The elasticity of the cell-like microdroplets was evaluated by a micropipette aspiration system as reported previously [52]. The surface elasticity (Young's modulus), E, is derived from the linear relationship between the elongation length into the micropipette, ΔL, and the aspiration pressure, ΔP : $E = (3\Delta P R_p \Phi/2\pi)/\Delta L$, wherein R_p and Φ are the micropipette inner radius and wall function, which is derived from the shape of the micropipette. We used a micropipette with an R_p smaller than × 0.4 of the microdroplet radius R. The value of Φ is 2.0. An increase in ΔL to above 50 μm under a very small ΔP (<< 0.5 kPa) indicates that the microdroplet is in liquid phase. In the case of the elastic gel phase, a linear relationship between ΔL and ΔP was confirmed for the small deformation within ΔL < 5 μm and ΔP < 3 kPa. Under these conditions, we derived the values of E. The temperature was approximately 25°C.

Acknowledgements

We are grateful to Tetsuro Hirose for providing the plasmid for FUS-Venus expression, and Tokiko Saigo for experimental assistance. Computations were partially performed on the NIG supercomputer at ROIS National Institute of Genetics.

References

1. Keilin D. The problem of anabiosis or latent life: history and current concept. Proc R Soc London Ser B, Biol Sci. 1959;150: 149–191.

2. Møbjerg N, Halberg KA, Jørgensen A, Persson D, Bjørn M, Ramløv H, et al. Survival in extreme environments - on the current knowledge of adaptations in tardigrades. Acta Physiol (Oxf). 2011;202: 409–420. doi:10.1111/j.1748-1716.2011.02252.x

3. Jönsson KI, Rabbow E, Schill RO, Harms-Ringdahl M, Rettberg P. Tardigrades survive exposure to space in low Earth orbit. Curr Biol. 2008;18: 729–731. doi:10.1016/j.cub.2008.06.048

4. Persson D, Halberg KA, Jørgensen A, Ricci C, Møbjerg N, Kristensen RM. Extreme stress tolerance in tardigrades: Surviving space conditions in low earth orbit. J Zool Syst Evol Res. 2011;49: 90–97. doi:10.1111/j.1439-0469.2010.00605.x

5. Sakurai M, Furuki T, Akao KI, Tanaka D, Nakahara Y, Kikawada T, et al. Vitrification is essential for anhydrobiosis in an African chironomid, Polypedilum vanderplanki. Proc Natl Acad Sci U S A. 2008;105: 5093–5098. doi:10.1073/pnas.0706197105

6. Clegg JS. The origin of threhalose and its significance during the formation of encysted dormant embryos of Artmia salina. Comp Biochem Physiol. 1965;14: 135–143. doi:10.1016/0010-406X(65)90014-9

7. Madin KAC, Crowe JH. Anhydrobiosis in nematodes: Carbohydrate and lipid metabolism during dehydration. Exp Zool. 1975;193: 335–342.

8. Erkut C, Penkov S, Khesbak H, Vorkel D, Verbavatz JM, Fahmy K, et al. Trehalose renders the dauer larva of caenorhabditis elegans resistant to extreme desiccation. Curr Biol. 2011;21: 1331–1336. doi:10.1016/j.cub.2011.06.064

9. Jain NK, Roy I. Effect of trehalose on protein structure. Protein Sci. 2009;18: 24–36. doi:10.1002/pro.3

10. Hengherr S, Heyer AG, Köhler HR, Schill RO. Trehalose and anhydrobiosis in tardigrades - Evidence for divergence in responses to dehydration. FEBS J. 2008;275: 281–288. doi:10.1111/j.1742-4658.2007.06198.x

11. Hara Y, Shibahara R, Kondo K, Abe W, Kunieda T. Parallel evolution of trehalose production machinery in anhydrobiotic animals via recurrent gene loss and horizontal transfer. Open Biol. 2021;11: 200413. doi:10.1098/rsob.200413

620 12. Hand SC, Menze MA, Toner M, Boswell L, Moore D. LEA proteins during water stress: Not just for
621 plants anymore. Annu Rev Physiol. 2011;73: 115–134. doi:10.1146/annurev-physiol-012110-142203
622 13. Goyal K, Walton LJ, Tunnacliffe A. LEA proteins prevent protein aggregation due to water stress.
623 Biochem J. 2005;388: 151–157. doi:10.1042/BJ20041931
624 14. Belott C, Janis B, Menze MA. Liquid-liquid phase separation promotes animal desiccation tolerance.
625 Proc Natl Acad Sci U S A. 2020;117: 27676–27684. doi:10.1073/pnas.2014463117
626 15. Hashimoto T, Horikawa DD, Saito Y, Kuwahara H, Kozuka-Hata H, Shin-I T, et al. Extremotolerant
627 tardigrade genome and improved radiotolerance of human cultured cells by tardigrade-unique protein.
628 Nat Commun. 2016;7: 12808. doi:10.1038/ncomms12808
629 16. Yamaguchi A, Tanaka S, Yamaguchi S, Kuwahara H, Takamura C, Imajoh-Ohmi S, et al. Two novel
630 heat-soluble protein families abundantly expressed in an anhydrobiotic tardigrade. PLoS One. 2012;7:
631 e44209. doi:10.1371/journal.pone.0044209
632 17. Boothby TC, Tapia H, Brozena AH, Piszkiewicz S, Smith AE, Giovannini I, et al. Tardigrades use
633 intrinsically disordered proteins to survive desiccation. Mol Cell. 2017;65: 975–984.
634 doi:10.1016/j.molcel.2017.02.018
635 18. Arakawa K, Numata K. Reconsidering the “glass transition” hypothesis of intrinsically unstructured
636 CAHS proteins in desiccation tolerance of tardigrades. Mol Cell. 2021;81: 409–410.
637 doi:10.1016/j.molcel.2020.12.007
638 19. Fletcher DA, Mullins RD. Cell mechanics and the cytoskeleton. Nature. 2010;463: 485–492.
639 doi:10.1038/nature08908.Cell
640 20. Pegoraro AF, Janmey P, Weitz DA. Mechanical properties of the cytoskeleton and cells. Cold Spring
641 Harb Perspect Biol. 2017;9: a022038. doi:10.1101/cshperspect.a022038
642 21. Hering L, Bouameur JE, Reichelt J, Magin TM, Mayer G. Novel origin of lamin-derived cytoplasmic
643 intermediate filaments in tardigrades. Elife. 2016;5: e11117. doi:10.7554/eLife.11117
644 22. Goldman RD, Khuon S, Chou YH, Opal P, Steinert PM. The function of intermediate filaments in cell
645 shape and cytoskeletal integrity. J Cell Biol. 1996;134: 971–983. doi:10.1083/jcb.134.4.971
646 23. Peter A, Stick R. Evolutionary aspects in intermediate filament proteins. Curr Opin Cell Biol. 2015;32:
647 48–55. doi:10.1016/j.ceb.2014.12.009

24. Tolleter D, Jaquinod M, Teyssier E, Payet N. Structure and function of a mitochondrial late embryogenesis abundant protein are revealed by desiccation. 2007;19: 1580–1589. doi:10.1105/tpc.107.050104

25. Koubaa S, Bremer A, Hincha DK, Brini F. Structural properties and enzyme stabilization function of the intrinsically disordered LEA_4 protein TdLEA3 from wheat. Sci Rep. 2019;9: 1–11. doi:10.1038/s41598-019-39823-w

26. Yoshida Y, Koutsovoulos G, Laetsch DR, Stevens L, Kumar S, Horikawa DD, et al. Comparative genomics of the tardigrades Hypsibius dujardini and Ramazzottius varieornatus. PLoS biology. 201715: e2002266. doi:10.1371/journal.pbio.2002266

27. Guo M, Pegoraro AF, Mao A, Zhou EH, Arany PR, Han Y, et al. Cell volume change through water efflux impacts cell stiffness and stem cell fate. Proc Natl Acad Sci U S A. 2017;114: E8618–E8627. doi:10.1073/pnas.1705179114

28. Kato M, Han TW, Xie S, Shi K, Du X, Wu LC, et al. Cell-free formation of RNA granules: Low complexity sequence domains form dynamic fibers within hydrogels. Cell. 2012;149: 753–767. doi:10.1016/j.cell.2012.04.017

29. Herrmann H, Aebi U. Intermediate filaments : structure and assembly. Cold Spring Harb Lab Press. 2016;8: a018242. doi:10.1101/cshperspect.a018242

30. Fasman PYC and GD. Prediction of protein conformation. Biochemistry. 1974;13: 222–245. doi:10.1295/kobunshi.34.978

31. Harmon TS, Holehouse AS, Rosen MK, Pappu R V. Intrinsically disordered linkers determine the interplay between phase separation and gelation in multivalent proteins. Elife. 2017;6: 1–31. doi:10.7554/eLife.30294

32. Jumper J, Evans R, Pritzel A, Green T, Figurnov M, Ronneberger O, et al. Highly accurate protein structure prediction with AlphaFold. Nature. 2021;596: 583–589. doi:10.1038/s41586-021-03819-2

33. Mirdita M, Ovchinnikov S, Steinegger M. ColabFold - Making protein folding accessible to all. bioRxiv [Preprint]. 2021; 2021.08.15.456425. Available from: https://www.biorxiv.org/content/10.1101/2021.08.15.456425v1 doi: 10.1101/2021.08.15.456425

34. Protter DSW, Parker R. Principles and properties of stress granules. Trends Cell Biol. 2016;26: 668–679. doi:10.1016/j.tcb.2016.05.004

677 35. Franzmann TM, Alberti S. Protein phase separation as a stress survival strategy. Cold Spring Harb
678 Perspect Med. 2019;9: 1–18. doi:10.1101/cshperspect.a034058
679 36. LeBlanc BM, Hand SC. Target enzymes are stabilized by AfrLEA6 and a gain of α-helix coincides with
680 protection by a group 3 LEA protein during incremental drying. Biochim Biophys Acta - Proteins
681 Proteomics. 2021;1869: 140642. doi:10.1016/j.bbapap.2021.140642
682 37. Tsuboyama K, Osaki T, Matsuura-Suzuki E, Kozuka-Hata H, Okada Y, Oyama M, et al. A widespread
683 family of heat-resistant obscure (Hero) proteins protect against protein instability and aggregation. PLoS
684 Biol. 2020;18: e3000632. doi:10.1371/journal.pbio.3000632
685 38. Horikawa DD, Kunieda T, Abe W, Watanabe M, Nakahara Y, Yukuhiro F, et al. Establishment of a
686 rearing system of the extremotolerant tardigrade Ramazzottius varieornatus : A new model animal for
687 astrobiology. Astrobiology. 2008;8: 549–556. doi:10.1089/ast.2007.0139
688 39. Mészáros B, Erdös G, Dosztányi Z. IUPred2A: Context-dependent prediction of protein disorder as a
689 function of redox state and protein binding. Nucleic Acids Res. 2018;46: W329–W337.
690 doi:10.1093/nar/gky384
691 40. Bailey T and, Elkan C. Fitting a mixture model by expectation maximization to discover motifs in
692 biopolymers. Proc Int Conf Intell Syst Mol Biol. 1994;2: 28–36.
693 41. Drozdetskiy A, Cole C, Procter J, Barton GJ. JPred4: A protein secondary structure prediction server.
694 Nucleic Acids Res. 2015;43: W389–W394. doi:10.1093/nar/gkv332
695 42. Lupas A, Van Dyke M, Stock J. Predicting coiled coils from protein sequences. Science (80-).
696 1991;252: 1162–1164. doi:10.1126/science.252.5009.1162
697 43. Pettersen EF, Goddard TD, Huang CC, Meng EC, Couch GS, Croll TI, et al. UCSF ChimeraX: Structure
698 visualization for researchers, educators, and developers. Protein Sci. 2021;30: 70–82.
699 doi:10.1002/pro.3943
700 44. Mi H, Ebert D, Muruganujan A, Mills C, Albou LP, Mushayamaha T, et al. PANTHER version 16: A
701 revised family classification, tree-based classification tool, enhancer regions and extensive API. Nucleic
702 Acids Res. 2021;49: D394–D403. doi:10.1093/nar/gkaa1106
703 45. Zhou Y, Zhou B, Pache L, Chang M, Khodabakhshi AH, Tanaseichuk O, et al. Metascape provides a
704 biologist-oriented resource for the analysis of systems-level datasets. Nat Commun. 2019;10: 1523.
705 doi:10.1038/s41467-019-09234-6

706 46. Kim D, Paggi JM, Park C, Bennett C, Salzberg SL. Graph-based genome alignment and genotyping
707 with HISAT2 and HISAT-genotype. Nat Biotechnol. 2019;37: 907–915. doi:10.1038/s41587-019-
708 0201-4
709 47. Liao Y, Smyth GK, Shi W. FeatureCounts: An efficient general purpose program for assigning sequence
710 reads to genomic features. Bioinformatics. 2014;30: 923–930. doi:10.1093/bioinformatics/btt656
711 48. Love MI, Huber W, Anders S. Moderated estimation of fold change and dispersion for RNA-seq data
712 with DESeq2. Genome Biol. 2014;15: 1–21. doi:10.1186/s13059-014-0550-8
713 49. Bindels DS, Haarbosch L, Van Weeren L, Postma M, Wiese KE, Mastop M, et al. MScarlet: A bright
714 monomeric red fluorescent protein for cellular imaging. Nat Methods. 2016;14: 53–56.
715 doi:10.1038/nmeth.4074
716 50. Sama RRK, Ward CL, Kaushansky LJ, Lemay N, Ishigaki S, Urano F, et al. FUS/TLS assembles into
717 stress granules and is a prosurvival factor during hyperosmolar stress. J Cell Physiol. 2013;228: 2222–
718 2231. doi:10.1002/jcp.24395
719 51. Tanaka S, Tanaka J, Miwa Y, Horikawa DD, Katayama T, Arakawa K, et al. Novel mitochondria-
720 targeted heat-soluble proteins identified in the anhydrobiotic tardigrade improve osmotic tolerance of
721 human cells. PLoS One. 2015;10: e0118272. doi:10.1371/journal.pone.0118272
722 52. Sakai A, Murayama Y, Fujiwara K, Fujisawa T, Sasaki S, Kidoaki S, et al. Increasing elasticity through
723 changes in the secondary structure of gelatin by gelation in a microsized lipid space. ACS Cent Sci.
724 2018;4: 477–483. doi:10.1021/acscentsci.7b00625
725
726

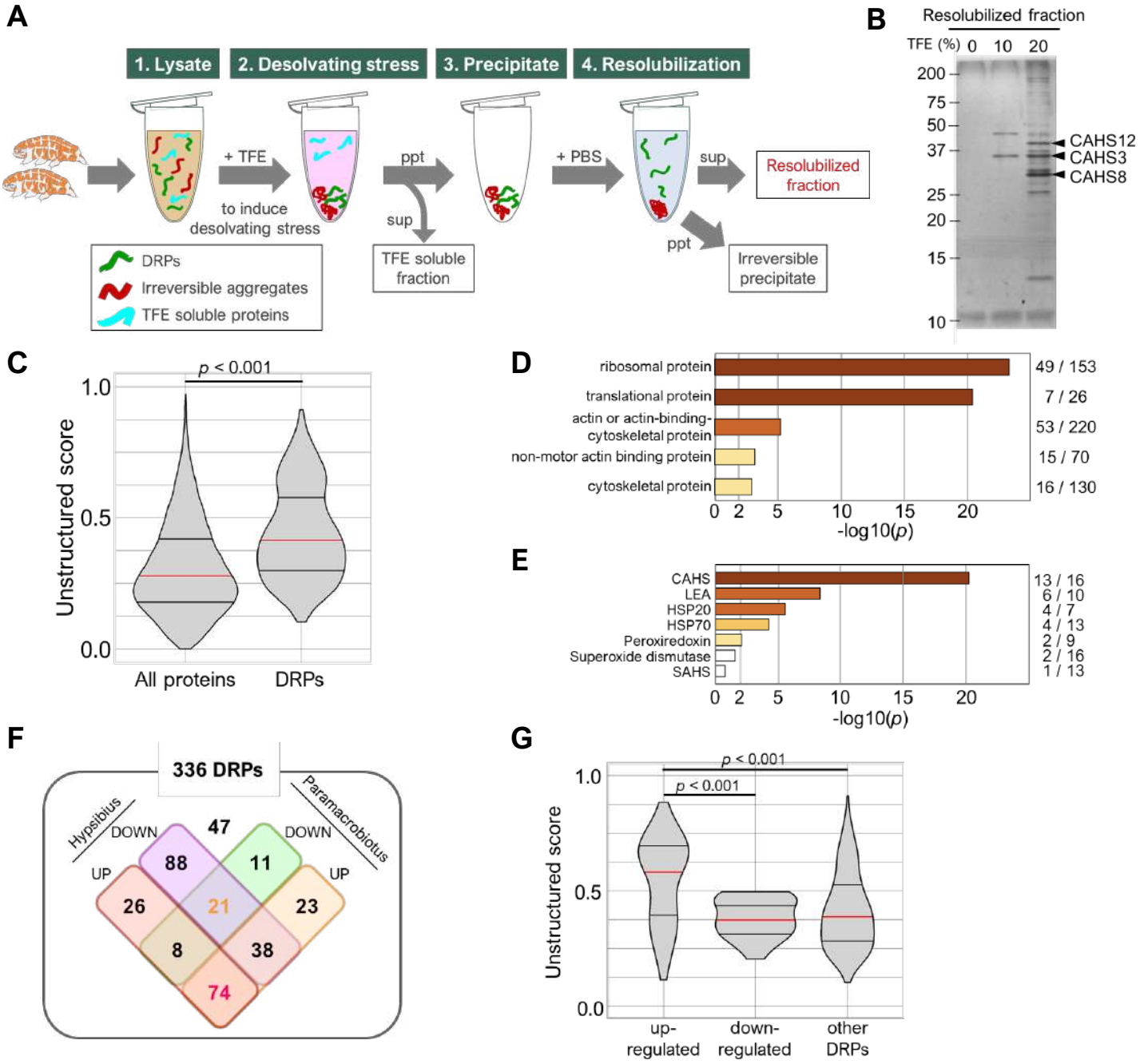

Fig 1. Isolation and characterization of dehydration-dependent reversibly condensing proteins (DRPs). (A) Experimental scheme of DRP isolation from tardigrade lysate. (B) SDS-PAGE image of resolubilized fractions with 0%, 10%, or 20% TFE treatment. (C) Comparison of the unstructured-score distributions between all tardigrade proteins and DRPs. (D) Enrichment analysis of the Panther protein class in DRPs. Ribosomal proteins and cytoskeletal proteins were significantly enriched. The numbers of the corresponding proteins detected in DRPs and all tardigrade proteomes are shown on the right, respectively. (E) Enrichment analysis of stress-related proteins in DRPs. CAHS proteins were significantly enriched in DRPs. (F) Venn diagram of DRPs classified by up- or down-regulation upon desiccation in orthologs of 2 other tardigrade species. (G) Comparison of unstructured-score distributions among the differently regulated protein groups in DRPs. “up-regulated” and “down-regulated” indicate up-regulated or down-regulated proteins in both species, respectively. Proteins up-regulated upon desiccation exhibited higher unstructured scores. Red and 2 black horizontal bars in violin plot indicate the 50th, 25th, and 75th percentiles, respectively. Statistical analyses were performed with the Wilcoxon rank sum test in (C) and Steel-Dwass test in (G).

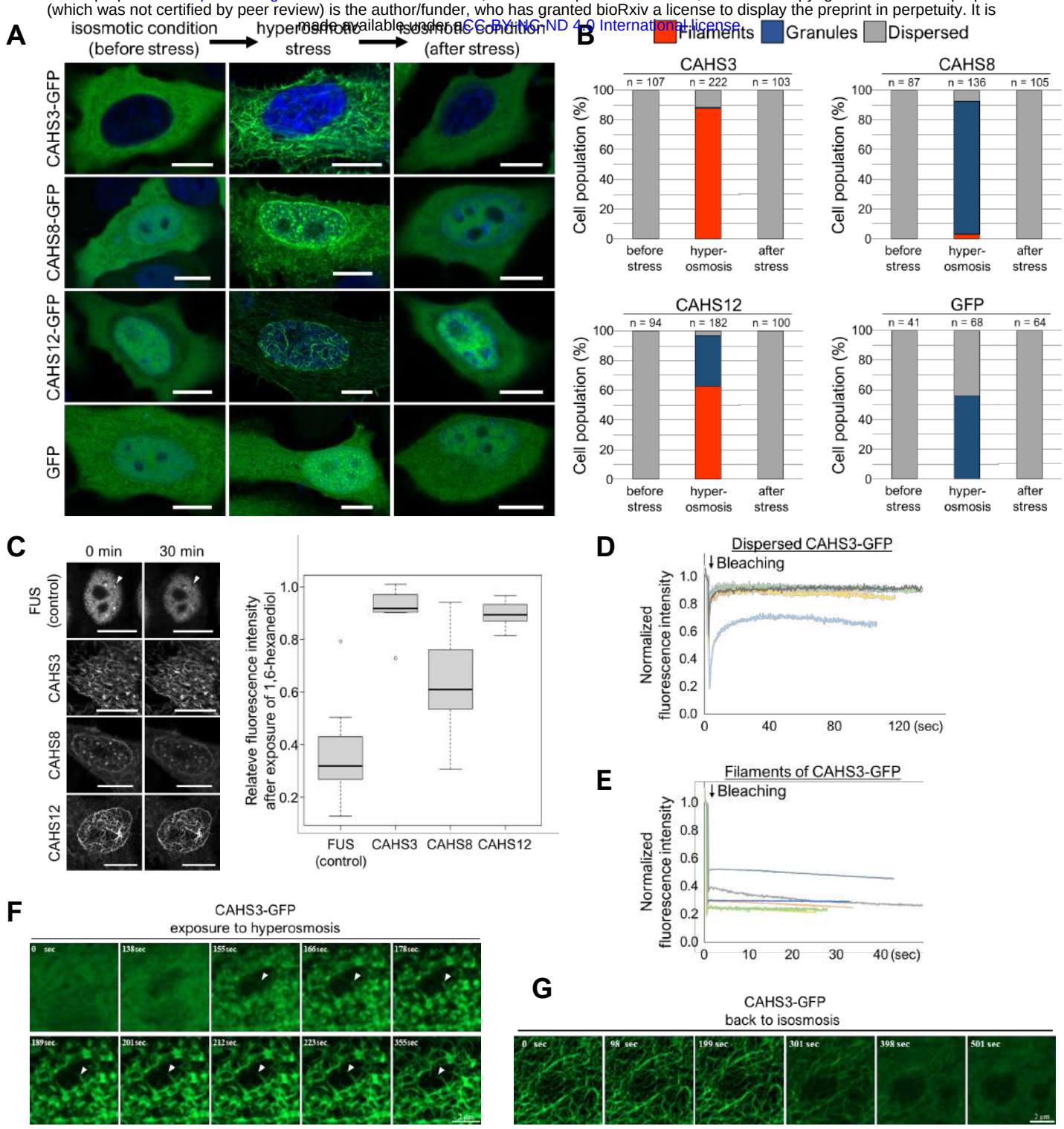

Fig 2. Reversible formation of filaments or granules by CAHS3, CAHS8, and CAHS12 proteins in response to a hyperosmotic stress. (A) Distribution changes in AcGFP1-tagged CAHS3, CAHS8, or CAHS12 proteins in HEp-2 cells during the transient hyperosmotic treatment in which the cells were exposed to HBSS containing 0.4 M trehalose. Blue indicates Hoechst33342 staining of nuclei. Scale bar, 10 μm. (B) The proportion of distribution patterns (filaments, granules, or dispersed) of each CAHS protein in human cells. (C) Effects of the liquid droplet disruptor, 1,6-hexanediol on condensates of FUS (n = 15), CAHS3 (n = 7), CAHS8 (n = 24), and CAHS12 (n = 7). FUS is a control protein sensitive to 1,6-hexanediol. Box plots show the distributions of the fluorescence intensity at 30 min relative to that at 0 min. Center bar and edges indicate 50th, 25th, and 75th percentiles, respectively and whiskers correspond to the 1.5 interquartile range. Scale bar, 10 μm. (D and E) Fluorescence recovery after photobleaching (FRAP) analyses of CAHS3-GFP in human cells in dispersed state under an isosmotic condition (D, n = 7), and in a filament-formed state under a hyperosmotic condition (E, n=6). (F and G) Time-lapse images of filament formation or deformation of CAHS3-GFP in human cells (see also S1 and S2 Movies). (F) CAHS3-GFP first condensed into granules (155 s) and then elongated into filaments (355 s). (G) CAHS3-GFP filaments simultaneously collapsed and dispersed (398 s). Time since the medium exchange to hyperosmotic (F) or isosmotic (G) solution is shown in each image. Scale bar, 2 μm.

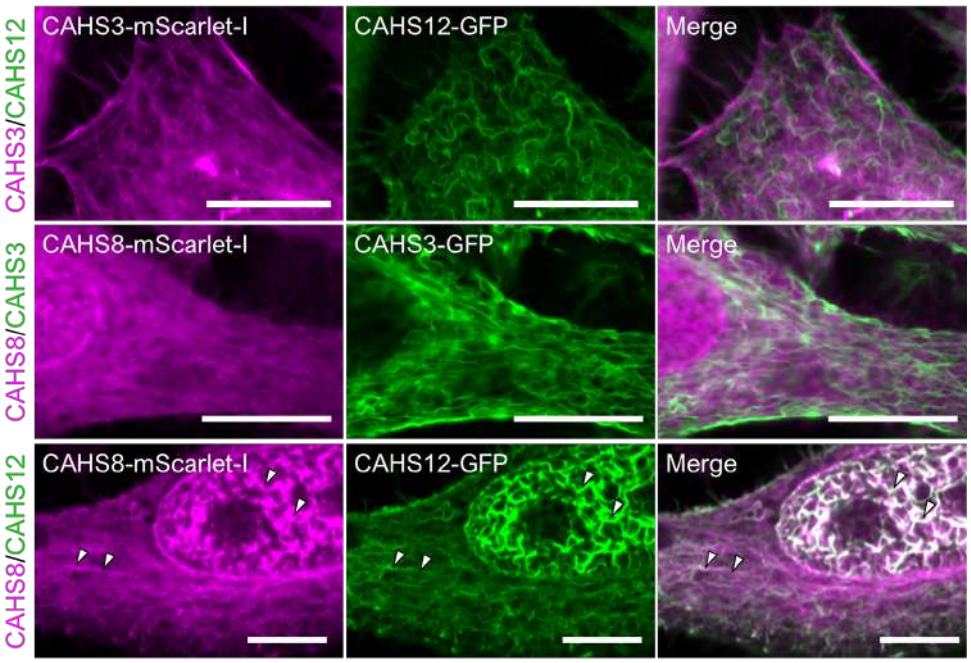

Fig 3. Cooperative filament formation of CAHS8 with CAHS12. Fluorescent images of HEp-2 cells co-expressing pairs of CAHS3, CAHS8, and CAHS12 proteins with a different fluorescent-tag under a hyperosmotic condition. CAHS3 co-localized with neither CAHS8 nor CAHS12. In contrast, CAHS8 well co-localized with CAHS12 filaments. White arrowheads indicate representative co-localization. Scale bar, 10 μm.

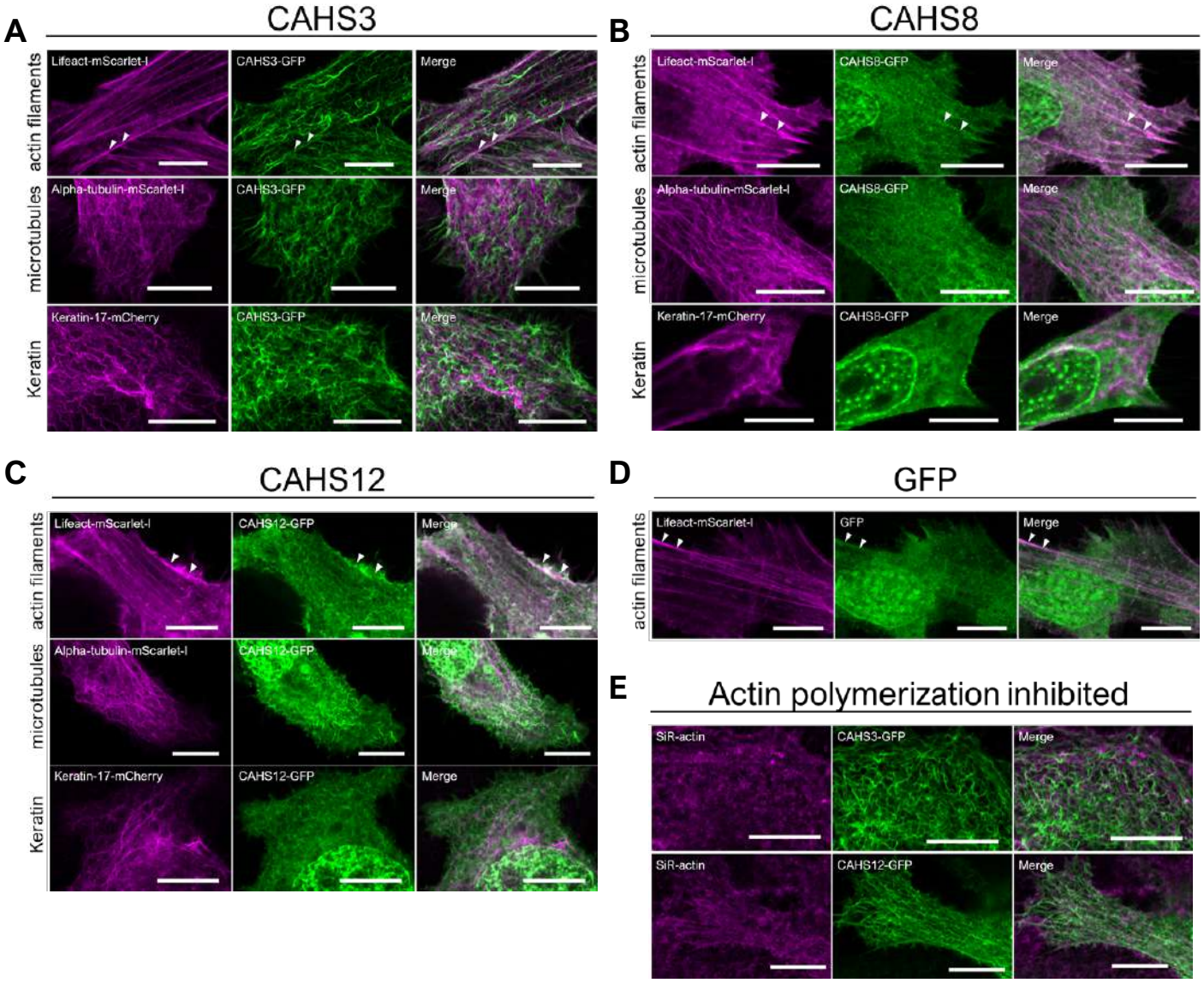

Fig 4. CAHS filaments are independent structures of other cytoskeletons. (A–C) Confocal images of AcGFP1-tagged CAHS proteins and fluorescently labeled cytoskeletal proteins in HEp-2 cells under a hyperosmotic condition. White arrows indicate slight co-localization of CAHS proteins and actin filaments. (D) Co-localization analysis of GFP alone and actin filaments. GFP alone partly co-localized with actin filament under a hyperosmotic condition. (E) Effects of the actin polymerization inhibitor cytochalasin B on CAHS filaments. Depolymerization of actin filaments had no effect on the formation of CAHS filaments. Scale bar, 10 μm.

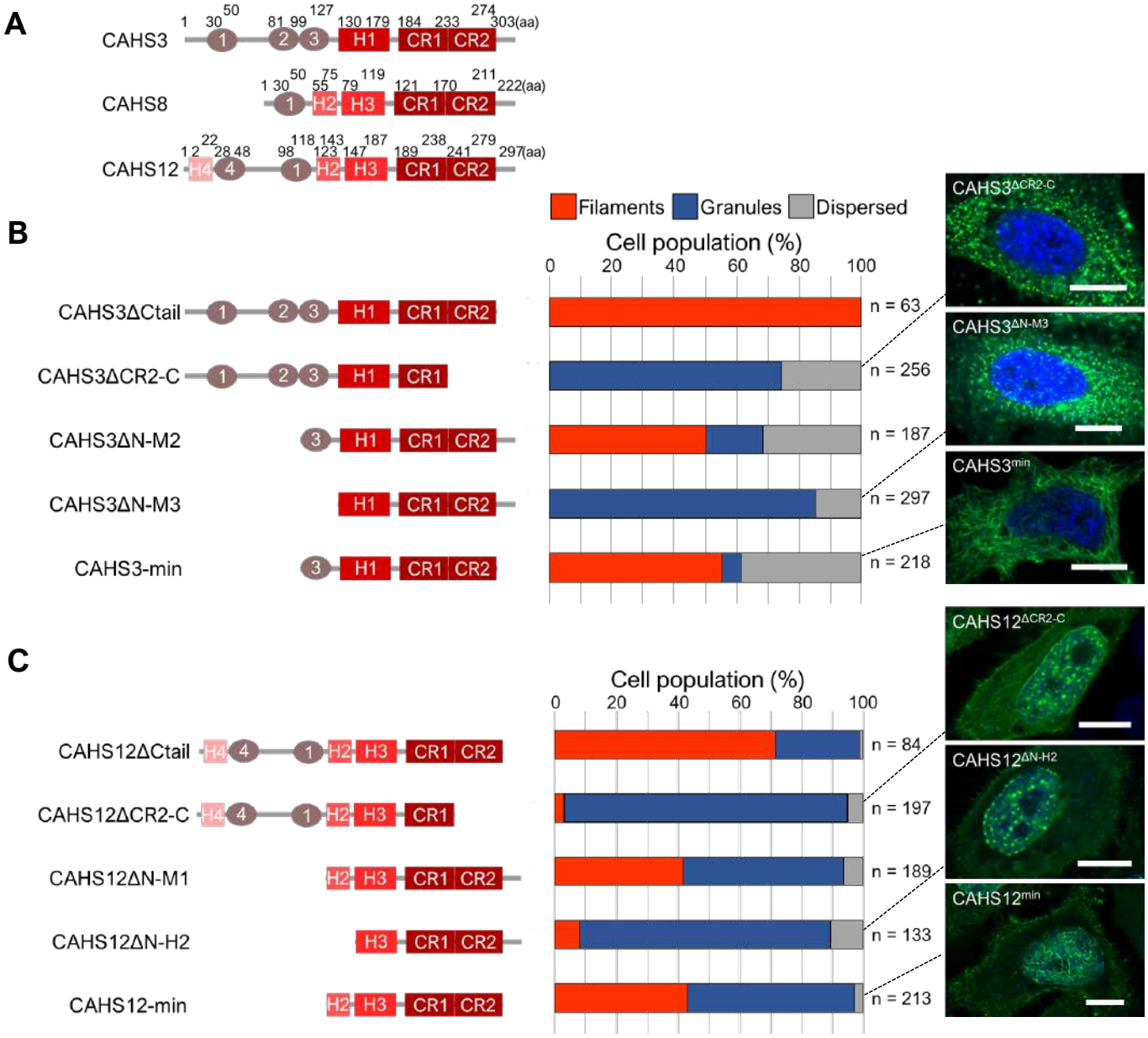

Fig 5. Conserved C-terminal regions are necessary and sufficient for the filament formation of CAHS3 and CAHS12. (A) Schematic diagrams of CAHS3, CAHS8 and CAHS12 proteins. “CR1” and “CR2” indicate putative helical motifs highly conserved among almost all CAHS family members. “H1”, “H2”, “H3”, and “H4” indicate putative helical conserved motifs. “1”, “2”, “3”, and “4” indicate other conserved motifs. (B and C) Schematic diagrams and the corresponding distribution patterns of the truncated mutants of CAHS3 (B) or CAHS12 (C). Quantified cell proportions of the distribution patterns under a hyperosmotic condition are shown as a stacked bar graph. Confocal images are shown for the representative distribution pattern of the corresponding CAHS mutants. Blue indicates Hoechst33342 staining of nuclei. Scale bar, 10 μm.

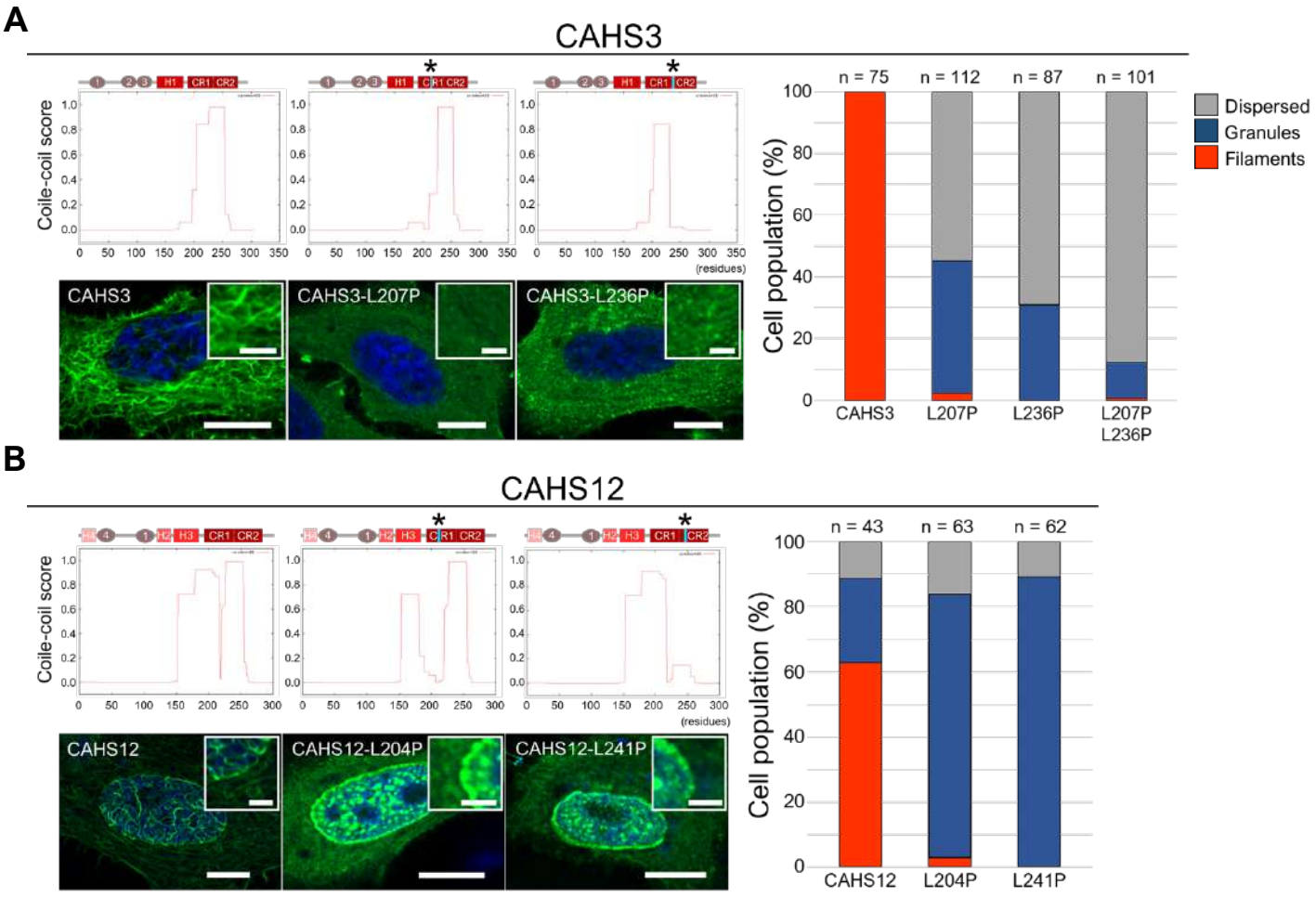

Fig 6. Suppression of filament-formation by mutations disrupting the coiled-coil structure in the conserved region of CAHS3 and CAHS12. (A and B) Effects of a helix-disrupting mutation by substituting leucine with proline on filament formation are shown for CAHS3 (A) and CAHS12 (B). Schematic structure and the coiled-coil score predicted by COILS are shown for both wild-type and proline substitution mutants. Asterisks indicate the sites of proline substitutions. Substitution with proline substantially decreased the coiled-coil score in the corresponding region. Confocal images show representative distribution patterns of the corresponding CAHS proteins (Scale bar, 10 μm). Enlarged image is shown as superimposition in each panel (Scale bar, 2.5 μm). Blue indicates Hoechst33342 staining of nuclei. Quantified cell proportions of each distribution pattern are shown as a stacked bar plot on the right.

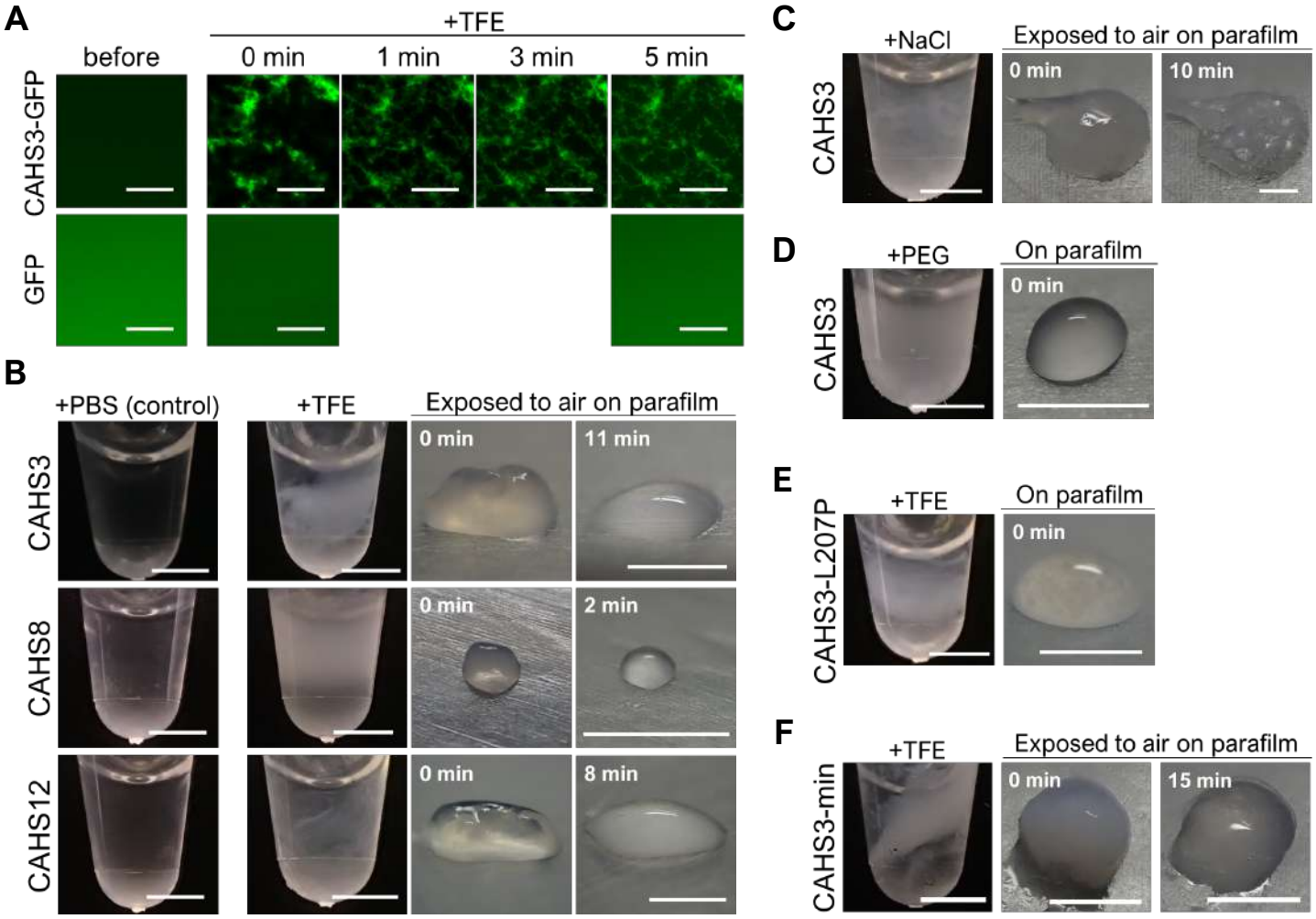

Fig 7. Gel transition of CAHS proteins upon desolvating or salt stress *in vitro*. (A) *In vitro* time-lapse confocal images of fibril formation of CAHS3-GFP proteins (1.24 mg/mL) after adding TFE (final 20%). GFP is a non-filament forming control. (B) TFE-dependent reversible gel-formation of CAHS proteins. By adding TFE (final 20%), CAHS3, CAHS8, and CAHS12 protein solutions (4.0 mg/mL) became turbid and transited into a gel-like state. The gels spontaneously liquefied within several minutes (shown in white letters) after exposure to air. (C) Persisting gelation of CAHS3 induced by the addition of NaCl (2 M). (D) Addition of the molecular crowding agent, polyethylene glycol (PEG, final 20%) induced turbidity, but no gelation. (E) Filament-defective CAHS3-L207P mutant protein solutions failed to transit into a gel-like state under 20% TFE. (F) Minimum filament-forming CAHS3 truncated protein (CAHS3-min) solution reversibly solidified under 20% TFE like full-length CAHS3 protein. Scale bar, 20 μm in (A), 2 mm in (B–F)

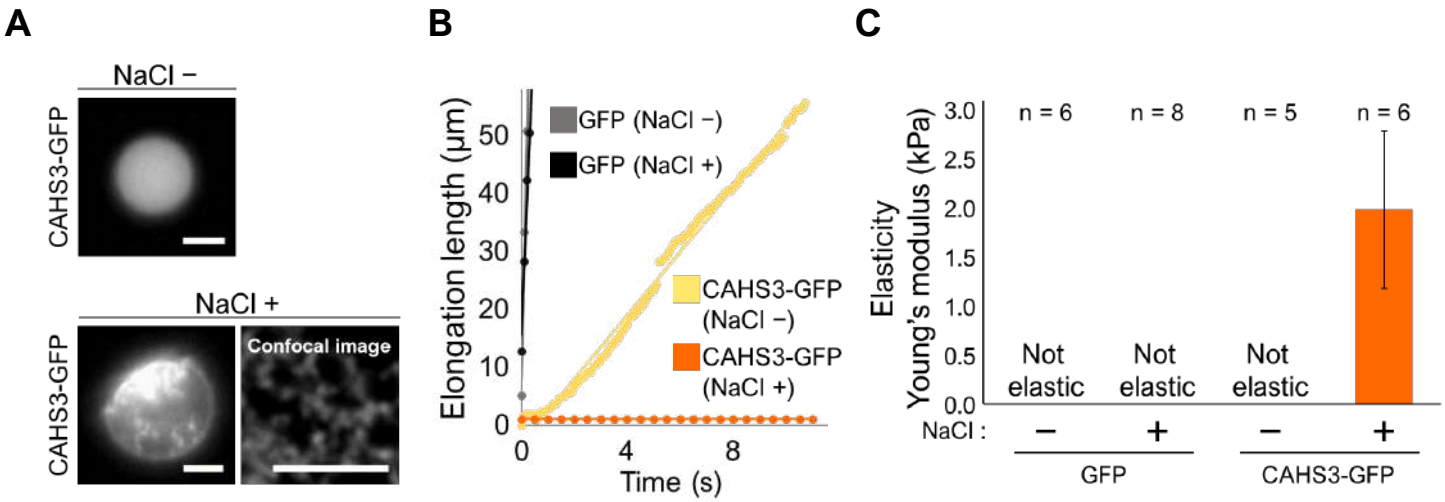

Fig 8. CAHS gelation increases the mechanical strength of cell-like microdroplets. (A) Representative fluorescent images of a microdroplet containing CAHS3-GFP in the absence or presence of additional NaCl. Scale bar, 5 μm. (B) Representative response curves of the elongation length of microdroplets containing CAHS3-GFP or GFP alone under a very small pressure (<< 0.5 kPa). Continuous elongation exceeding 50 μm indicates not elastic and in a liquid phase. (C) Comparison of the elasticity (Young's modulus) among droplets containing CAHS3-GFP or GFP with or without NaCl addition. Data are presented as average ± SE.